Supporting information

Acoustofluidic focusing and separation of rare tumor cells using transparent lithium niobate transducers†

Zezheng Wu, [a] Hongqiang Jiang, [b] Lingling Zhang, [a] Kezhen Yi, [c] Heng Cui, [a] Fubing Wang, [c] Wei Liu, [a] Xingzhong Zhao, [a] Fuling Zhou, [b] and Shishang Guo,* [a]

[a] Key Laboratory of Artificial Micro- and Nano-structures of Ministry of Education, School of Physics and Technology, Wuhan University, Wuhan 430072, P. R. China

[b] Department of Hematology, Zhongnan Hospital of Wuhan University, Wuhan, Hubei 430072, P. R. China

[c] Department of Laboratory Medicine, Zhongnan Hospital of Wuhan University, Wuhan, Hubei 430072, P. R. China

Physical material properties of some materials in acoustic devices.

In the bulk acoustic wave (BAW) devices, the formation of standing wave is usually generated through the harder wall reflection. Thus, considering the acoustic attenuation in wall reflection, acoustic impedance (Z) is introduced to evaluate it. For example, the acoustic impedance of PMMA is slightly higher than that of water. As a result, when acoustic wave propagates to the interface of the water and PMMA, much acoustic wave will transmit past the interface and the rest will reflect to form standing wave in the resonant cavity. By contrast, acoustic wave is almost reflected when it propagates to the interface of the water and harder materials, like glass. Therefore, the

absorption of sound energy caused by polymer will result in decreasing the sound pressure and effectiveness when manipulating micro-particles. The acoustic impedances of some materials are shown in Table S1. Additionally, acoustic impedance is calculated by the equation of $Z = \rho c$, where ρ and c are density and speed of sound, respectively.

Table S1 Physical material properties of some materials.[1]

Materials	Density ($kg\ m^{-3}$)	Speed of sound ($m\ s^{-1}$)	Characteristic acoustic impedance ($\times 10^6\ pa \cdot s\ m^{-3}$)
Silicon	2330	8430	19.6
Pyrex-glass	2330	5500	12.8
PMMA	1150	2590	3.0
Water	1000	1490	1.5

Fusion bonding

Three pieces of glass processed via laser would be used to make the device. Firstly, the glassed were washed with detergent, acetone, anhydrous ethanol and deionized water for 3 to 5 min. And then, the clean glasses were sealed under flowing deionized water to ensure that there are no bubbles between each piece of glass. The sealed glasses were baked at 80 ℃ for 1 to 2 hours for pre-bonding. At the procedure, it should be observed whether there were diffraction rings between the glass plates.

As a result, unless there were no diffraction rings near the micro channels, the glass plates should be disassembled and clean again for next bond.

After accomplishing the above steps, the sealed glass plates needed to be baked at higher temperature for stronger bonding, which followed the Table S2.

Table S2 The temperature program of fusion bonding.

Serial numbers	Temperature	Time (min)
0	50	1
1	100	11
2	100	71
3	540	171
4	540	291
5	50	391
6	50	0 (end)

The temperature curves of 36° LNO and PZT

The temperature was characterized by a small hand-held temperature sensor. And when the sine single was added on the LNO (20 mm × 5 mm×1 mm) and PZT (20 mm × 10 mm×1 mm), respectively, the flowing velocity was controlled to be 400μL h^{-1}, the temperature of PZT was over 40 °C with 1min while that of LNO increased extremely slowly. The power added on PZT and LNO were 36 dBm and 32 dBm, respectively for manipulating the PS particles. And the various power added on LNO was tested to observe the change of temperature which showed in Fig. S1.

Although, when the power added on LNO was equal to that on PZT, the temperature of LNO was less than that on PZT. It exhibits that LNO produces far less heat than PZT on account of the inherent property of single crystal materials.

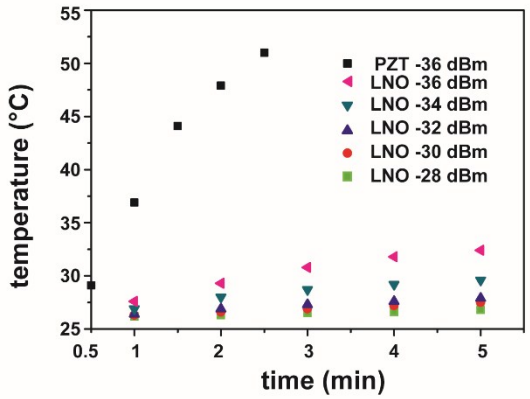

Fig. S1 The temperature of PZT and LNO when acoustic single was on. The temperature of PZT was higher than that of LNO.

Finite element simulation of the device

The resonance of the whole device was simulated, including the whole micro-channel, shown in Fig. S5. And the result of simulation in y- and z- direction was also supplemented in Fig. S2. Usually, the acoustic radiation force on small particles was governed by eqn (1),[2]

$$F_{rad} = -\frac{4\pi}{3}a^3\nabla\left[f_1\frac{1}{2}k_0\langle p_1^2\rangle - f_2\frac{3}{4}\rho_0\langle v_1^2\rangle\right] \quad (1a)$$

$$f_1 = 1 - \frac{K_p}{K_0} \quad (1b)$$

$$f_2 = \frac{2\left(\frac{\rho_p}{\rho_0} - 1\right)}{2\frac{\rho_p}{\rho_0} + 1} \quad (1c)$$

Where f is the frequency, K_0 is the compressibility of fluid and, K_p is the compressibility of particle, p_1 is the pressure field and v_1 is the velocity field. And ρ_p and ρ_0 are the density of particle and fluid, respectively.

A glass chip with a piece of 36° LNO attached to the chip was considered to simulate the distribution in the micro channel. A ac voltage was applied to the piezoelectric element (36° LNO), and when it vibrates, a time-harmonic ultrasound pressure field $p_1 exp(-iwt)$, w is the angle frequency. The pressure field p_1 and velocity field v_1 in the chip and the microchannel are governed by Helmholtz wave equation,

$$\nabla^2 p_1 = -\frac{w^2}{c^2} p_1 \tag{2a}$$

$$v_1 = -\frac{i}{w\rho} \nabla p_1 \tag{2b}$$

Where c and ρ are the speed of sound and the density of the given material (Table S1), respectively.

In this work, considering surface normal vector at a boundary, three boundary conditions are employed: the hard wall condition, the soft wall condition and the continuity condition for pressure and velocity,[3]

$$n \cdot \nabla p_1 = 0, (hard\ wall) \tag{3a}$$

$$p_1 = 0, (soft\ wall) \tag{3b}$$

$$\frac{n \cdot \nabla p_1^{(a)}}{\rho_a} = \frac{n \cdot \nabla p_1^{(b)}}{\rho_b}, and\ p_1^{(a)} = p_1^{(b)}, (continuity) \tag{3c}$$

Considering the acoustic impedance of glass is larger than that of water, the glass could be treated as an infinitely hard material. That is $n \cdot \nabla p_1 = 0$.

In standing plane field,

$$F_a = 4\pi\varphi(f_1, f_2) k a^3 E_{ac} \sin(2kz) \tag{4a}$$

$$E_{ac} = \frac{p_a^2}{4\rho_0 c_0^2} \tag{4b}$$

$$p_a \propto U_{pp} \tag{4c}$$

$$E_{ac} = U_{pp}^2 \tag{4d}$$

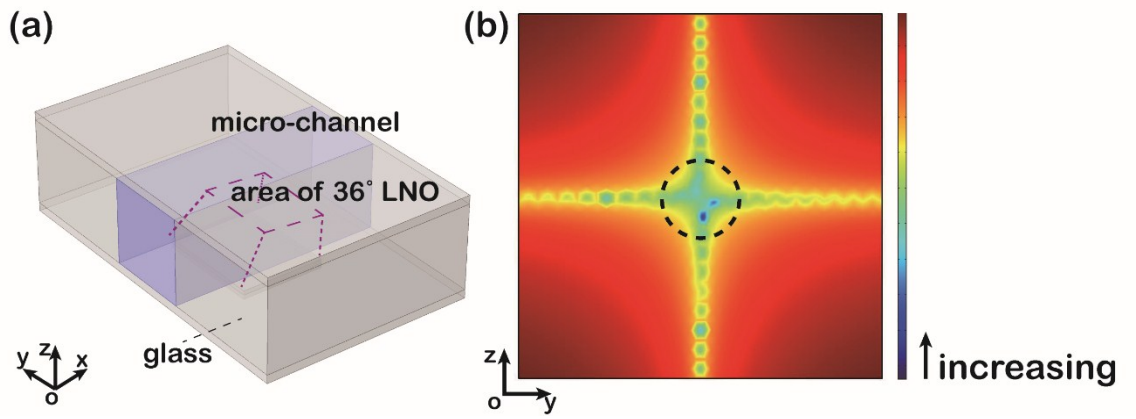

Fig. S2 The simulation result of acoustic pressure in y- and z- direction.

where E_{ac} is the acoustic energy density, and $\varphi(f_1,f_2)$ is the so-called acousto-phoretic contrast factor, which determines the direction of small particles. The factor z is the distance from pressure anti-node in the wave propagation axis, k is the wavenumber ($2\pi f/c_0$), p_a is the pressure amplitude, c_0 is speed of sound in fluid, and U_{pp} is the external voltage.

From the aforementioned equation, the value of E_{ac} plays an important role in determining the acoustic radiation force. Typically, in a typical low voltage ($U_{pp} \leq 10\ V$) in silicon/glass chips where PZ26 is usually acted as acoustic transducer, $E_{ac} = 10 - 100\ J\ m^{-3}$. At the experiment, the excited mode of 36° LNO is similar to PZ26, but the physical parameter of LNO is different from PZT. When external voltage (U_0) is applied to the upper and lower electrodes of piezoelectric materials, the axial motion u is considered by eqn (5),[4]

$$u(0) = U_0 \frac{ds_D}{2s_E} \frac{\tan(\frac{1}{2}k_{DL})}{\frac{1}{2}k_D - k^2 \tan(\frac{1}{2}k_D L)} \quad (5)$$

where d is charge constant; s_D, s_E is mechanical compliances; k^2 is the electromechanical coupling coefficient, which describes energy conversion of electrical and mechanical energy; L is the length along the vibrational direction; k_D is the wavenumber. The vibration amplitude and sound pressure (p_a) are positively correlated. And it is noted that the charge constant (d) of PZT is about two orders of magnitude higher that of 36° LNO, but the electromechanical coupling coefficient (k^2) of the single crystal LNO is higher. It is roughly estimated that acoustic radiation force excited by PZT is higher than that of LNO at a same typical voltage.

And in typical standing surface acoustic wave (SSAW) devices, likewise, the acoustic radiation force is governed by eqn (4), but the vibration amplitude is usually 0.1 – 10 nm. When it is also tested at a typical low voltage, the acoustic radiation force is lower than the typical bulk devices.

Optimizing of ratio of flow velocity in inlets

The width and height of the flow channel were both designed to be 200 μm, the pressure node would locate at the middle of the channel. At the experiment, in order

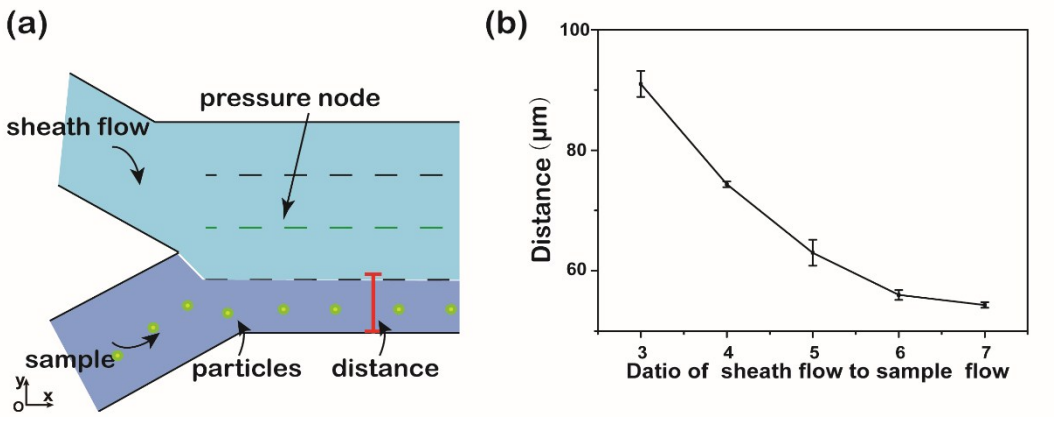

Fig. S3 Illustration of the state of two kinds of flow (DI water and absolute ethyl alcohol) within different ratio. (a) The structure of the two inlets shows that the fluid interface and the sample flow is hustled to the side wall. (b) Different ratios of two flows influence the distance.

to form a table laminar flow, the ratio of flow velocity in inlets was studied. And, DI water was injected into sheath flow inlet while another inlet was injected with absolute ethyl alcohol. As a result, when the ratio of flow velocity between sample flow to sheath flow was set to 1: 6, the particle would be pushed near to the side wall of the main channel and form a table laminar flow for next separation. As shown in Fig. S3, the width of sample flow mixing particles which has been pre-aligned was about 50 μm, and this provided sufficient conditions for lateral displacement of particles. It showed that when the ratio was 1: 5, the width of sample flow was narrow, and when 1: 7, it was hardly changed. Therefore, if not specified, the ratio of flow velocity was set to 1: 6 in all experiments.

cells distribution in outlets.

Some figures about the images of cells collected were added in Supporting information Fig. S4.

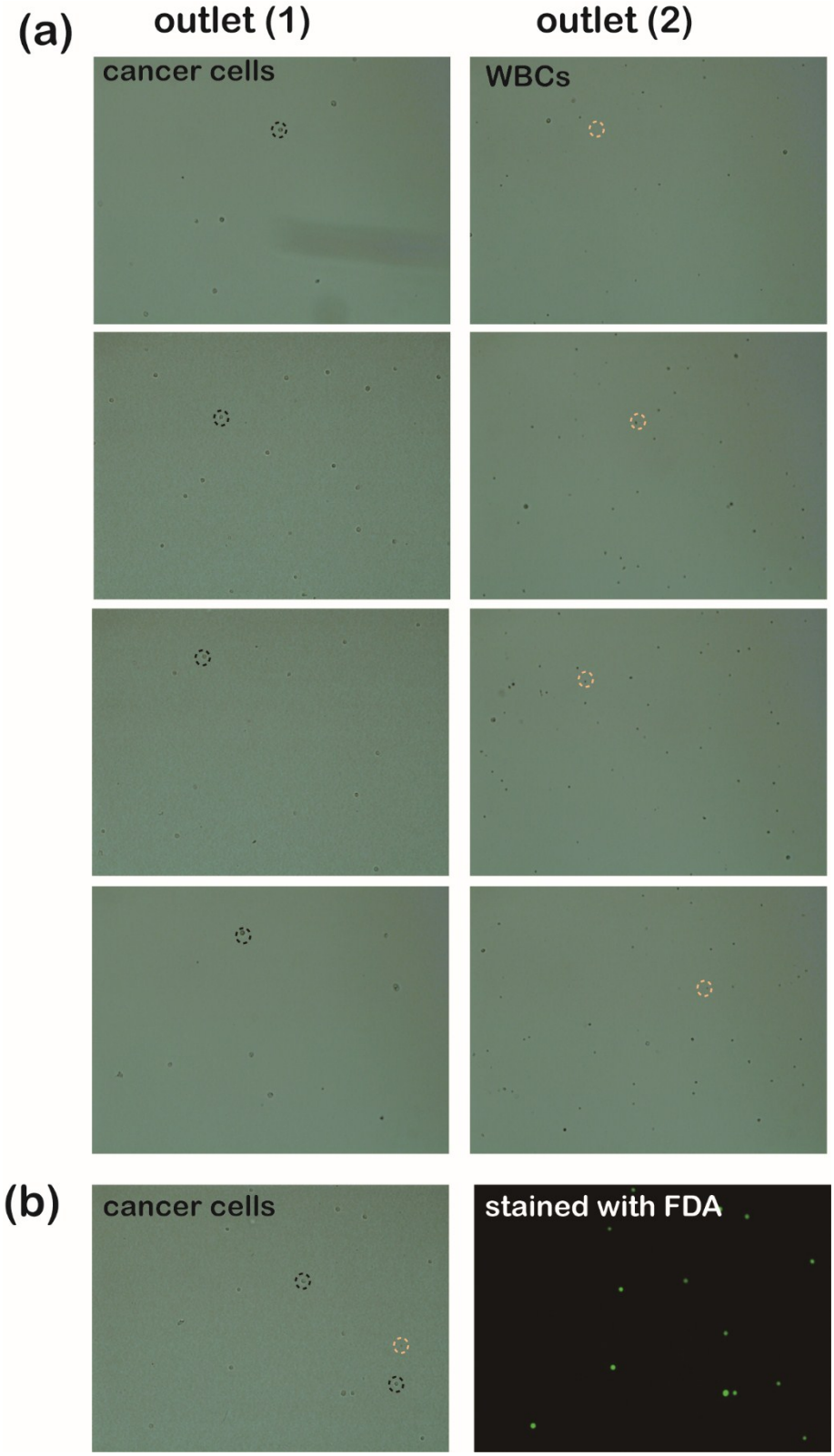

Fig. S4 The distribution of cells in outlets. (a)The cancer cells and WBCs were in different outlets. (b) Cancer cells were stained with FDA.

Reference:

(1) T. Laurell, F. Petersson and A. Nilsson, *Chem Soc Rev*, 2007, 36, 492-506.
(2) H. Bruus, *Lab Chip*, 2012, 12, 1014-1021.
(3) R. Barnkob, P. Augustsson, T. Laurell and H. Bruus, *Lab Chip*, 2010, 10, 563-570.
(4) J. Dual and D. Moller, *Lab Chip*, 2012, 12, 506-514.